Studtite formation assessed by Raman spectroscopy and ^{18}O isotopic labeling during the oxidative dissolution of a MOX fuel

Lola Sarrasin, Sandrine Miro, Christophe Jégou, Magaly Tribet, Véronique Broudic, Caroline Marques, Sylvain Peuget

Studtite formation assessed by Raman spectroscopy and ^{18}O isotopic labeling during the oxidative dissolution of a MOX fuel

L. Sarrasin, S. Miro, C. Jégou, M. Tribet, V. Broudic, C. Marques and S. Peuget

CEA, DES, ISEC, DE2D Univ. Montpellier, Marcoule, France

Keywords: oxidative dissolution, studtite, uranium peroxide, MOX MIMAS, UO_2, ^{18}O isotopic labeling, Raman spectroscopy

Abstract

The formation of studtite has been studied during the oxidative dissolution of a MIMAS MOX fuel disc in aerated water enriched in ^{18}O under a gamma radiation source, coupling Raman spectroscopy and solution analyzes. The use of isotopic labeling allowed following the reactions responsible for the precipitation of studtite. At the beginning of the experiment, different ^{18}O enrichments in the uranyl and peroxide bonds of the studtite were observed. While the uranyl bond was primarily enriched in ^{18}O, the peroxide bond contained large amounts of ^{16}O. This result suggests an oxygen contribution coming from different radiolytic species for each bond: H_2O_2 and radicals. The comparison with a UO_2 sample leached in similar conditions ruled out a role of the Pu alpha self-irradiation in this different behavior. Yet, the influence of the MOX MIMAS heterogeneous microstructure and chemistry is observed with the preferential dissolution of the UO_2 grains, the Pu-rich areas being much more stable with regard to the dissolution. In addition, the studtite first precipitates preferentially on the Pu-poor areas of the sample before covering the entire surface, including the plutonium-enriched aggregates, at the end of the experiment.

1. Introduction

Understanding the alteration mechanisms between water and damaged fuels remains essential in the context of incidental or even accidental scenarios.[1,2] Describing in particular the behavior of actinides under water and in the presence of an intense irradiation field is crucial to get closer to these incidental scenarios. These severe irradiation conditions could affect the speciation of actinides and therefore the fuel dissolution mechanisms by promoting oxidizing conditions by water radiolysis, the precipitation of U(VI) secondary phases and the release/retention of radionuclides.[3,4]

To date, the oxidative dissolution of UO_2 has been widely described in the literature as well as the nature of the uranium secondary phases, which are liable to precipitate.[5,6] Thus, in waters exhibiting simple chemistry, intense irradiation fields (alpha and or beta / gamma) lead to the formation of hydrogen peroxide by water radiolysis and to the precipitation of uranium peroxides. The formation of these peroxides has been the subject of numerous observations both on irradiated fuel[7–9] and on UO_2 model systems[10,11], whether or not submitted to irradiation, with or without addition of hydrogen peroxide into the solution[12,13]. The structure and properties of these peroxides (studtite, metatstudtite) are well known[14–17] and they can have different shapes and morphologies (needles, colloids and nanoclusters) depending precipitation conditions[18,19]. The resistance to irradiation of these compounds has also been the subject of recent developments[20,21].

Although many data are available on UO_2, knowledge of the dissolution mechanisms of MOX fuels is more limited[6,22–24] and the role of plutonium as well as the effects of microstructure requires further studies. Indeed, can the presence of plutonium affect the nature of the secondary phases and the oxidative dissolution process? Can local plutonium concentrations associated with fuel microstructure affect the

mechanisms? In order to answer these questions, an original experimental approach has therefore been implemented. It combines Mimas MOX fuel leaching experiments in pure labeled water ($H_2{}^{18}O$) under a strong gamma irradiation field to the characterization of the leached surfaces by Raman spectroscopy. The Raman spectroscopy, which has a spatial resolution of the order of 1 μm^3, remains a tool of choice for studying structural changes at the fuel surface[25]. Moreover, as vibrational spectroscopy, it remains sensitive to isotopic effects and can give information on the mechanisms of actinide oxidation and the formation of secondary phases. The use of isotopes also makes it possible to study the respective role of species produced by water radiolysis (radicals and molecular species) on the formation of uranyl ions and peroxide bonds. This subject remains debated in the literature[26,27] and relatively little studied through isotopic studies.

2. Materials and methods

2.1. Materials

MOX disc. An unirradiated MIMAS MOX fuel disc with an initial Pu/(U+Pu) ratio (in wt.%) of 7.39 was used for this study. The pellet was manufactured in June 2000 at MELOX plant (Marcoule, France) according to the MIMAS (MIcronization of a MASter blend) process. This manufacturing process results in heterogeneous samples composed of 3 distinct phases of different plutonium contents: Pu-rich agglomerates (~20 wt.% of Pu), Pu-poor agglomerates (often referred to as "UO_2 matrix", ~3 wt.% of Pu) and a coating phase of intermediate composition (~ 7 wt.% of Pu).[28]

A sintered disc of 8 mm in diameter and around 2 mm thick was mirror-polished on one side and annealed at 1100°C under an Ar/4%H_2 gas mixture for 5 hours to remove surface defects produced by the polishing process and restore the oxygen stoichiometry.

UO_2 disc. A depleted UO_2 disc, containing 0.25 at.% of ^{235}U, was also used in this study. It measures 8.2 mm in diameter and is 3 mm thick. One side of the sample was mirror polished and, just before the leaching experiment, the disc was annealed in the same conditions than the MOX sample.

2.2. Leaching experiment.

In order to remove any residual oxide layer at the surface, the pellet was subjected to 5 pre-leaching cycles in carbonated water ($[NaHCO_3] = 10^{-3}$ mol.L^{-1}) in which U(VI) strongly dissolves.[29] The release peak of U(VI) due to this potential oxide layer could indeed subsequently mask the effects of radiolysis during the leaching experiment.

The sample was leached for 79 days in a dedicated shielded cell. The pellet was first immerged in a leaching reactor filled with 230 mL of ^{18}O-enriched (97 atom % ^{18}O) deionized water (INNOVA-CHEM, France) at pH 4.89 ± 0.04 and placed on a gamma source (^{60}Co, at around 70 Gy/h). The reactor consists of a titanium dioxide liner (chemically inert) inserted in a stainless-steel body. An air vent located on the cap of the reactor generates oxidizing conditions that favor the formation of uranium peroxide/secondary phases during the experiment.[24] A picture and a schematic representation of the experimental set-up can be found in a previous publication.[24] The slightly acidic pH of the water, the aerated conditions and the gamma irradiation field enabled a simulation of the storage pools conditions.

A second experiment performed with a depleted UO_2 pellet in a similar aerated enriched water (98 at.% ^{18}O, INNOVA-CHEM) has been carried out so as to compare to the MOX results and thus study the impact of the MOX chemistry and microstructure on the leaching process. This leaching experiment, performed in similar conditions, lasted 27 days.

For each leaching experiment, the solution and the pellet's surface were regularly analyzed by sampling of the leachates and in-operando analysis of the sample surface by optical microscopy and Raman spectroscopy. Therefore, the pellets were regularly removed from the leaching reactor, then dried with a

wiper to remove any residual water and transferred to the adjacent hot cell in which the micro-Raman is located. At the end of the analysis (less than one day), the pellets were brought back to the leaching cell and placed into the leaching reactor to continue the leaching experiment.

2.3. Characterization techniques.

A nuclearized microscope, with 1.25x to 100x objectives (Optique Peter, France), is coupled through optic fibers to a Raman spectrometer LabRam HR 800 (Jobin-Yvon) located outside the cell. The spectrometer is equipped with a 532 nm Nd-YAG laser of 300 mW in combination with optical density filters to control the laser power on the sample.

In this study, a 600 grooves/mm grating was used, covering a range of 1711 cm^{-1} and giving a spectral resolution of 1.7 cm^{-1}. The laser was focused onto the sample using a 100x objective with a corresponding lateral resolution of around 1 µm. The laser power at the sample surface was limited to ~1 mW to avoid oxidation and phase transformation during the measurements. Individual spectra were obtained using an exposure time of 30 to 45 s and accumulated two to four times depending on the Raman response of the analyzed area of the sample. Raman mappings were also carried out with the z-axis autofocusing system. Labspec software (Horiba, UK) was used to process these Raman mappings. Before each Raman analysis, the spectrometer was calibrated with a silicon reference sample.

Solutions of hydrogen peroxide (~1 $mol.L^{-1}$) were analyzed by Raman spectroscopy outside the hot cell using a 1800 gr/mm grating. Spectra were recorded for 5 × 30 s by focusing the laser, using a 100x objective, inside a drop of solution deposited on a microscope slide.

In parallel, the leachate was regularly sampled and analyzed (H_2O_2 by UV-Vis, pH, dissolved U by KPA and Pu by radiometry) to follow the modification of the solution chemistry and the alteration of the sample. The techniques and experimental devices are detailed in previous publications.[3,24]

At the end of the experiment, the sample was analyzed by SEM-EDS on a Jeol 6300 equipped with BSE, SE and X-Rays detectors, using a 20 kV electron acceleration voltage. For the X-rays analysis, the oxygen K transition and the uranium and plutonium M transitions were used.

3. Results and discussion

A very quick alteration of the MOX sample was observed during the experiment. Thanks to a meticulous tracking, the monitoring of the same area over time by optical microscopy (after each transfer in the adjacent hot cell) allowed to study the evolution of this alteration (Figure 1). After only two days in the reactor, the surface of the MIMAS MOX sample was partially covered with significant amounts of precipitated phases (Figure 1b and 1e). An optical microscope examination of the precipitated zones revealed the presence of needle-like precipitates (insert in Figure 1e). These precipitates, identified as studtite, are localized on small circular zones of a few microns in diameter and are, on the contrary, absent of larges circular areas.

During the experiment, the precipitated layer gradually extends and thickens over the small circular areas as shown in Figure 1c and 1f. A thin layer appears almost on all the rest of the sample. This preferential precipitation is reminiscent of the heterogeneous microstructure of the MIMAS-MOX sample.

Raman spectroscopy and mappings were widely used to characterize this phase, the incorporation of ^{18}O, its correlation with the sample chemistry and evolution during the experiment. These characterizations of solid were combined with leachate analyzes to follow the alteration markers.

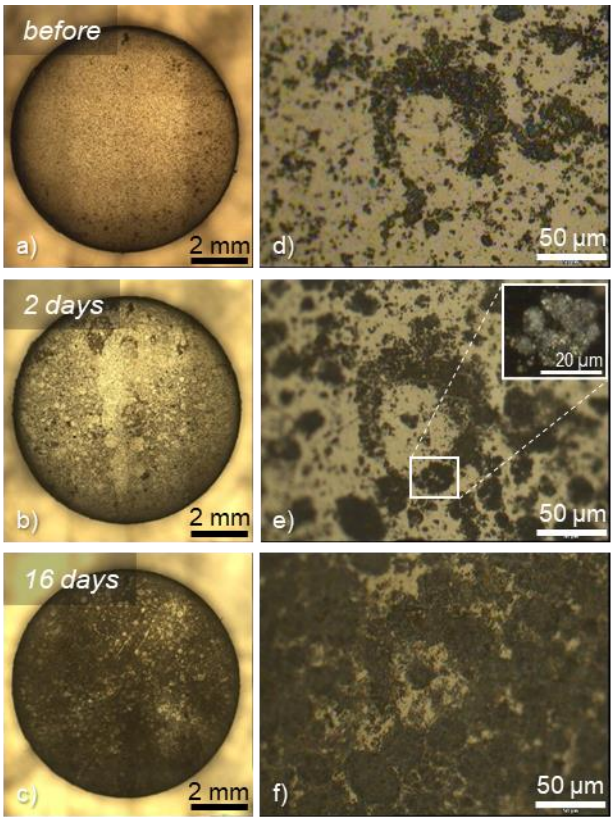

Figure 1 : a-c) Optical images reconstruction of the pellet's surface (5x, 24 images) and d-f) Optical micrograph observations (50x) of the same area before the leaching experiment, after 2 and 16 days of leaching. Insert: zoom in polarized light (100x)

3.1. Leaching solution analyzes results

The precipitation is associated to a significant dissolution of the fuel, observed by the monitoring of U and Pu concentrations in the leachate, and an important production of H_2O_2 due to the gamma irradiation field that produce radiolytic species responsible for the oxidative dissolution of the fuel. The peroxide concentration is around 10^{-4} mol.L^{-1}, in good agreement with previous studies which showed that [H_2O_2] tends towards 1.2×10^{4} mol.L^{-1}, concentration imposed by this gamma source under aerated conditions.[3,23] After reaching 1.5×10^{-6} mol.L^{-1} the first leaching days, the uranium concentration decreases down to 1.5×10^{-7} mol.L^{-1} indicating an uranium deposition. The pH remains quite stable during the experiment, around 4.7 ± 0.3. On the other hand, the plutonium released in solution increases continuously during the experiment, with a dissolution rate of 5.0×10^{-9} mol.L^{-1}.d^{-1} (from 3.8×10^{-9} mol.L^{-1} at day 2 to 3.5×10^{-7} mol.L^{-1} at day 72). These results indicate a continuous dissolution of the MOX sample accompanied by the precipitation of a uranium-based compound. These data are consistent with those already published under the same experimental conditions.[23,24] The strong oxidizing and slightly acidic conditions promote the high oxidation states for actinides (U(VI) and Pu(V)) and therefore their high release into the solution.

The solution chemistry is conducive to the formation of studtite, an uranium peroxide formed by chemical reaction between uranyl ions UO_2^{2+} and H_2O_2, both dissolved in the leachate. Usually, the solution must be highly oversaturated with respect to uranium to induce a massive precipitation of this phase at the fuel surface.[24] The Saturation Index (SI) can be calculated by considering the solution chemistry, the ionic activities product Q_{exp} and the solubility constant K_s (Eq. 1 and 2).

$$SI = log\frac{Q_{exp}}{K_S} \qquad (1)$$

$$Q_{exp} = \frac{[UO_2^{2+}][H_2O_2]}{[H^+]^2} \qquad (2)$$

The solubility constant for studtite is equal to $K_s = 1.37\times10^{-3}$ at room temperature[15] and the concentrations expressed are in $mol.L^{-1}$.

The saturation index is always positive and above 2 throughout the experiment, which shows that the solution is constantly over-saturated. From the first days, our experimental conditions were conducive to the formation of studtite, hence the important precipitation layer observed at the surface of the sample after 2 days.

3.2. Raman characterizations.

Raman spectroscopy confirmed the presence of studtite although its Raman spectrum differs from the one usually observed (Figure 2). Studtite has a monoclinic structure (C2/c) consisting of infinite linear chains of UO_2 units bonded to two oxygen peroxide groups (O_2^{2-}) in which the oxygen atoms are side bonded.[14] Between the chains are located four water molecules: two coordinated to the uranium atoms and two others hydrogen-bonded between the chains. The accurate formulation is $[UO_2(O_2).(H_2O)_2].2H_2O$. Studtite has two main Raman vibrational modes located at 819 cm^{-1} and 867 cm^{-1} that are attributed, respectively, to the symmetric stretching vibration of the uranyl bond (U=O) and to the stretching of the oxygen peroxide bond (O—O)[30], visible in the reference spectrum of studtite in the bottom of Figure 2.

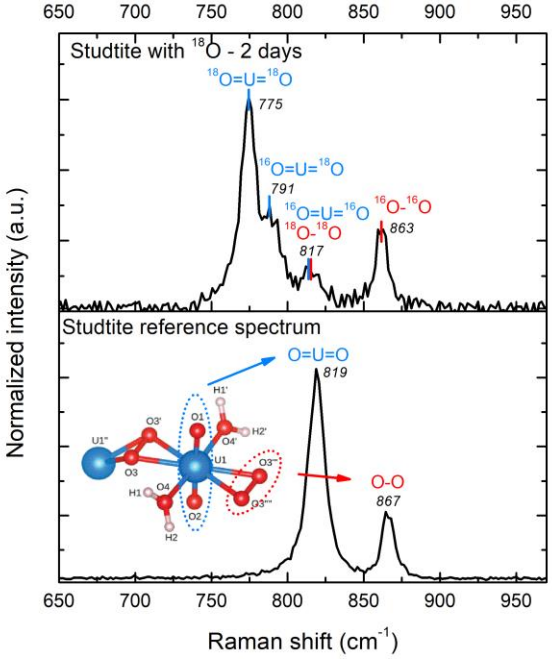

Figure 2 : Raman spectra of studtite formed at the surface of the MIMAS MOX sample after two leaching days in ^{18}O-enriched water (top) and formed in water of natural isotopic composition (bottom) with bands assignment and ball-and-stick representation [31].

The spectra of the studtite formed in ^{18}O-labeled water exhibits bands at 775, 791, 817 and 863 cm^{-1} (top of Figure 2). On some spectra, a small contribution is also visible at around 840 cm^{-1}. Observation of new bands in vibrational spectra after isotopic labeling is common and due to the substitution of specific atoms by their isotope in the analyzed compound. The new bands in the studtite spectrum certainly results from the incorporation of ^{18}O in the studtite structure. The spectrum exhibits two bands previously observed:

the peroxide band shifted at 863 cm^{-1} and the uranyl band located at 817 cm^{-1}, involving both only ^{16}O. The two additional bands centered at 775 and 791 cm^{-1} correspond, respectively, to the $^{18}O=U=^{18}O$ and $^{16}O=U=^{18}O$ configurations. A second band, attributed to the completely substituted peroxide bond, is overlapping the uranyl band at ~817 cm^{-1}.

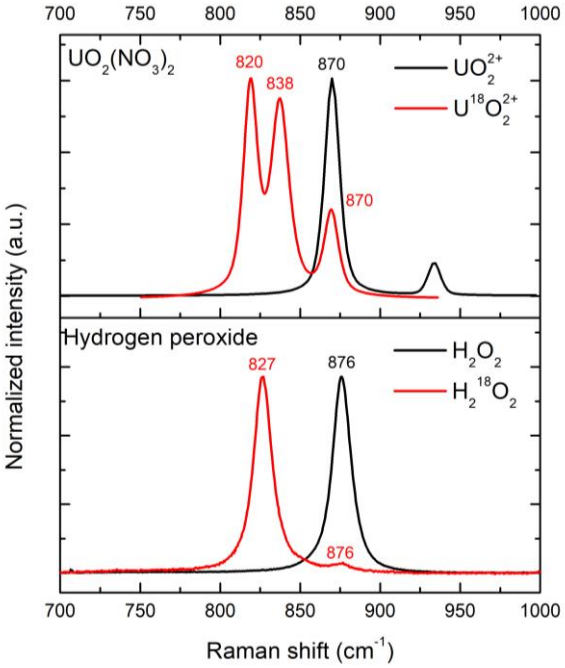

Figure 3 : Raman spectra of: top UO_2^{2+} [32](the peak at 933 cm^{-1} is due to the ClO_4^- internal standard) and $U^{18}O_2^{2+}$ [33]; bottom: H_2O_2 and $H_2{}^{18}O_2$ (enriched in 97% in ^{18}O) at 1M concentration analyzed during this study.

The band assignments of Figure 2 are supported by the Raman spectra of UO_2^{2+} and H_2O_2 enriched in ^{18}O (Figure 3) and by the calculation of the theoretical vibration frequencies (see next section). The free uranyl group UO_2^{2+} is linear and have a $D_{\infty h}$ symmetry. Group theory predicts four vibrational modes but only the uranyl symmetric stretching is Raman active and appears at 870 cm^{-1} [34] (black spectrum, top of Fig 3). Berger[33] studied the UO_2 dissolution mechanism in acidic media (HNO_3 diluted in $H_2{}^{18}O$) and followed the oxygen repartition in the dissolved UO_2^{2+} ions by Raman spectroscopy. The author observed a band triplet with the isotopic enrichment in ^{18}O, with bands located at 820, 838 and 870 cm^{-1} (red spectrum, top of Figure 3). They correspond to the splitting of the U=O band and are explained by the three isotopic configurations $^{18}O=U=^{18}O$, $^{16}O=U=^{18}O$ and $^{16}O=U=^{16}O$.

Although the Raman spectrum of ^{18}O-enriched UO_2^{2+} and our uranyl bands are similar in shape, their vibration frequencies differ. In fact, the uranyl ion is very sensitive to its environment and its symmetric stretching vibration frequency can be located between a wide range of wavenumbers [800 and 900]cm^{-1} [35,36] depending on the functional group it is bonded to (carbonate, sulfate, peroxide…). In our study the band triplet shift is due to the peroxide ligand and is in good agreement with the studtite band positions as the $^{16}O=U=^{16}O$ band is located at ~817 cm^{-1}.

To assess the isotopic effect of the peroxide bond, a solution of hydrogen peroxide enriched in 18-oxygen (2-3% $H_2{}^{18}O_2$ in H_2O with 97% ^{18}O, Sigma Aldrich) was analyzed by Raman spectroscopy. The spectrum of H_2O_2 on the [700-1000] cm^{-1} range presents one unique sharp and intense peak located at 876 cm^{-1} (black spectrum, bottom of Figure 3).[37] When enriched with 97% of 18-oxygen the peak shifts to 827 cm^{-1} (red spectrum, bottom of Figure 3). A small peak is still present at 876 cm^{-1} with an intensity equal to 3% of the

main peak. This is consistent with the enrichment given by the manufacturer and confirms that the isotopic substitution induces a splitting of the peroxide band in two bands. The studtite spectra agree with these results that evidence different Raman responses for the peroxide and uranyl bonds enriched in oxygen 18.

It is noteworthy that Bastians *et al.* also observed a splitting of some of their Raman bands when analyzing studtite samples.[30] A shouldering appears with the symmetric stretching band of the uranyl bond at around 815 cm^{-1} and one with the stretching band of the peroxide bond at around 840 cm^{-1}. According to the authors, this splitting may arise from the correlation effects between the uranyl and studtite symmetries. The shouldering at 840 cm^{-1} may fit our experimental data but, contrary to the authors, we could not evidence such bands while studying the spectra of the studtite formed in non-enriched water (Figure 2). It could also arise from a $^{16}O/^{18}O$ mixing associated to the peroxide bond but, considering the $H_2{}^{18}O_2$ spectrum and the low intensity of the band when visible in our spectra, we choose to neglect it.

The splitting of Raman bands with the isotopic substitution is a phenomenon usually observed in liquids rather than solids. In solids, the isotopic effect manifests through a global shift of the Raman bands.[38] However a splitting of Raman bands has also been observed in uranium peroxide cage clusters.[39] Although the spectrum of studtite nanoclusters is quite different from our studtite spectra, this study highlights that a Raman band splitting may be observed when analyzing small free studtite entities. This result raises questions about the size of probed studtite entities and their arrangement in the precipitated layers, not covered in this paper.

3.3. Isotopic enrichment modelling and evolution through time

The peak positions as well as their relative intensities reflect the distribution of the ^{18}O in the molecule. Their modelling thus allows to follow the isotopic repartition in the studtite and track down the reaction mechanisms and the oxygen exchanges between the leachate and the species formed during the experiment.

The theoretical vibration frequencies associated with each of the different oxygen configurations of the studtite bonds can be evaluated using the harmonic oscillator frequency formula. (Eq. 3), for symmetric stretching, assuming that k remains constant with the isotopic substitution.

$$\nu = \frac{1}{2\pi c}\sqrt{\frac{k}{\mu}} \qquad (3)$$

Where ν is the vibration frequency, k is the force constant of the bond and μ is the reduced mass.

According to the formula, the vibrational frequency of an atomic bond is inversely proportional to the masses of the atoms bonded and is reduced for heavier atoms. The maximal shift induced by the isotopic substitution of the oxygen 16 by the oxygen 18 should be of 47 cm^{-1} for the uranyl bond and 50 cm^{-1} for the peroxide bond. Experimental and calculated bands positions values are reported in Table 1. This calculation gives very good results for the H_2O_2 position but is less accurate for the other values as they are inserted in the studtite crystal and because the $^{16}OU^{18}O$ bands are more difficult to calculate due to the asymmetric repartition of the oxygen masses.[33] This calculation still gives a good approximation of the bands position, which supports the studtite band assignment.

Table 1: Calculated and experimental Raman bands positions of the 18-oxygen enriched H_2O_2, UO_2^{2+} and studtite spectra

Bond	Compound	Configuration	Experimental position	Calculated position
Peroxide	*H_2O_2*	*$^{16}O^{16}O$*	*876 (1)*	-
		$^{18}O^{18}O$	*827 (1)*	*826*
	Studtite	$^{16}O^{16}O$	863 (1)	-
		$^{18}O^{18}O$	817 (2)	814
Uranyl	*UO_2^{2+}*	*$^{16}OU^{16}O$*	*870 (3)*	-
		$^{16}OU^{18}O$	*838 (3)*	*844*
		$^{18}OU^{18}O$	*820 (3)*	*820*
	Studtite	$^{16}OU^{16}O$	817 (2)	-
		$^{16}OU^{18}O$	791 (2)	793
		$^{18}OU^{18}O$	775 (1)	770

The three uranyl peaks intensity should follow a binomial distribution. Their intensities are directly proportional to the probability of a given isotopic configuration which, itself, depends on the isotopic abundance in oxygen 16 (x) and oxygen 18 (~1-x). Their respective probabilities are x^2 for $^{16}OU^{16}O$, $2x(1-x)$ for $^{16}OU^{18}O$ and $(1-x)^2$ for the $^{18}OU^{18}O$ peak. Using this model, we were able to determine the isotopic abundance in the uranyl bond from the intensity ratio of the uranyl bands. The oxygen content in the peroxide bond, that splits into two bands, is then deduced from the band's intensity ratio in a second time. The fit results and mean isotopic enrichments (average of different acquisitions on the sample surface) of both bonds are indicated on each graph (Figure 4) with associated standard deviation.

After two leaching days, the uranyl bond can be adjusted considering an isotopic enrichment in ^{18}O of 87±1 % while the peroxide bond contains 27±6 % of ^{18}O (top of Figure 4a). At the beginning of the experiment the isotopic exchange is already almost complete between the solution and the uranyl bond but is partial in the peroxide bond. The studtite formed is therefore mainly enriched in 18-oxygen in the uranyl bond and 16-oxygen in the peroxide bond.

This isotopic enrichment evolves with the leaching time: the uranyl bands remain almost unchanged while the peroxide band at 817 cm^{-1} ($^{18}O^{18}O$) increases to the detriment of the 863 cm^{-1} band ($^{16}O^{16}O$) (Figure 4). The fit indicates that the peroxide ^{18}O enrichment tends to equalize the uranyl one. It reaches a ^{18}O content after 16 days of 72±5 % and contains at the end of the experiment (41 days) 84±1% of ^{18}O against 87±1% for the uranyl bond.

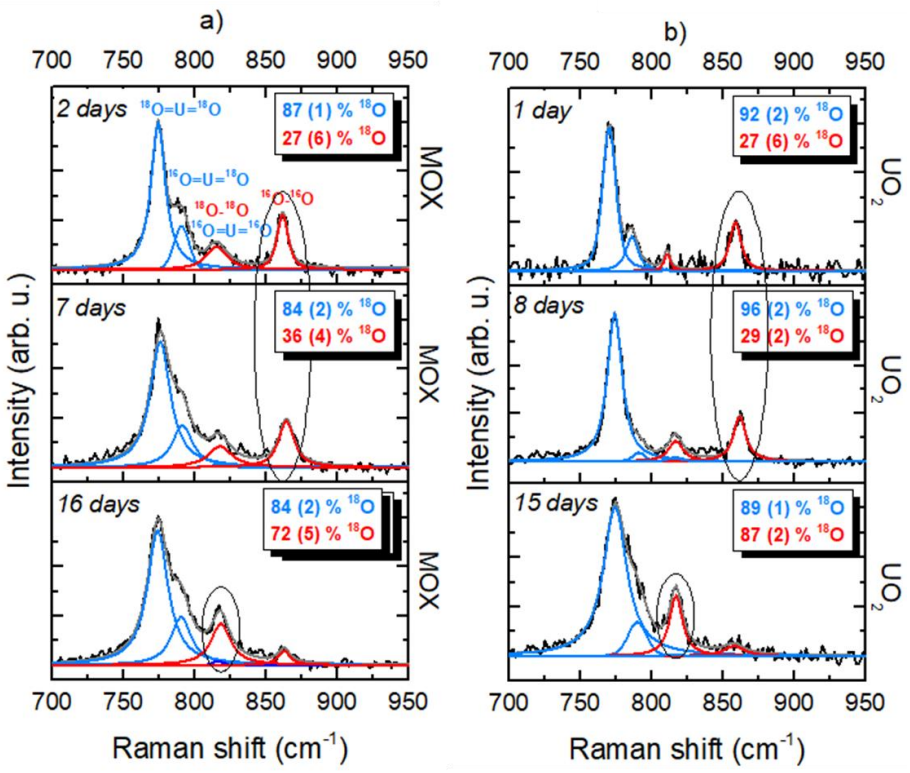

Figure 4 : Evolution through time of the studtite spectra for: a) a MOX sample compared to b) a UO_2 sample. The mean isotopic enrichment of the uranyl (blue) and peroxide (red) bonds are indicated on each graph with the standard deviation in parentheses.

These results show a change in the reaction with time that may be attributable to several mechanisms: a modification of the precipitation mechanisms, a change in the reactive species or an isotopic exchange with the solution. However, previous studies seem to indicate that once formed the isotopic exchange between the solution and the uranyl ions[33,40], the hydrogen peroxide[41] or the studtite[42] is limited. The presence of plutonium in the MOX sample may explain this behavior change. Indeed, the alpha particles irradiation of the Pu agglomerates may be responsible for the local production (range of 40 µm in water[24]) of different radiolytic products, such as $H_2{}^{18}O_2$, that could increase the quantity of ^{18}O in the peroxide bond.

To evaluate the influence of the alpha radiation field from the Pu agglomerates, a leaching experiment was performed on a UO_2 disc. The Raman spectra of both experiments are presented in Figure 4. For clarity purpose, the dates on which the UO_2 sample was examined were chosen to be as close as possible to those of the MOX sample.

The comparison of the Raman spectra of both experiments revealed a similar behavior. For the UO_2 sample the uranyl bond contains initially 92±2% of ^{18}O against 27±6% for the peroxide bond. The intensity of the bands does not evolve much during the first week of the experiment (day 1 to 8) but increases greatly for the ^{18}O-^{18}O peroxide band after two weeks (analysis at day 15). This change is visible in Figure 4 where the main contribution to the peroxide bond is circled. The kinetic and isotopic enrichment are very close from those of the MOX sample. This similarity in behavior between the (U, Pu)O_2 and UO_2 matrices tends to show that the local alpha irradiation of the Pu-rich agglomerates of the MOX sample has no major impact on the studtite formation mechanisms, and is not responsible for spectral changes over time in ^{18}O enriched water.

3.4. Heterogeneous precipitation

By analyzing various precipitation sites at the surface of the MOX sample by Raman spectroscopy, it appears that the studtite signal is often associated with that of the UO_2 matrix with a generally low T_{2g} mode located at 445 cm^{-1} as well as a 2LO mode at 1150 cm^{-1}, as visible on the red spectrum on Figure 5. By performing Raman mappings of the surface, it was therefore possible to correlate the studtite layer to the U-rich areas. Indeed, when following the $2LO/T_{2g}$ area ratio on the sample surface, which is very intense in U-rich areas and tends to zero in the Pu-rich areas, over the studtite bands areas ([700-900]cm^{-1} range), we can see a match between both signals (Figure 5c). On the contrary, the studtite signal is absent from the rest of the sample at day 2. These areas are characterized by a T_{2g} mode shifted towards higher wavenumbers, corresponding to a higher plutonium content. For example, on the spectrum extracted from the black part of the optical picture presented in Figure 5 (blue spectrum), a T_{2g} mode located at 448 cm^{-1} is observed which indicates a Pu content of around 10%, corresponding to the mean Pu enrichment of the coating phase. No precipitation is either observed on the high Pu-content areas, characterized by a T_{2g} mode at 452 cm^{-1}, corresponding to a 20% Pu-content. These plutonium concentrations correspond to the values determined in the literature for the coating phase[43,44] and the Pu agglomerates[28] of MIMAS MOX pellets. The studtite precipitation is therefore linked to the local chemistry of the sample and, while it covers the UO_2 zones, it is absent from the areas with intermediate to high Pu content (coating phase and Pu-rich agglomerates).

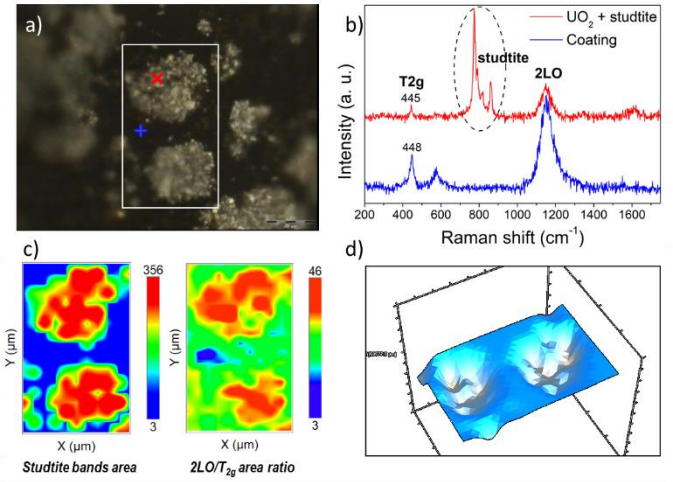

Figure 5 : Raman analysis of the MIMAS-MOX surface after 2 leaching days; a) Optical picture in polarized light (100x); b) Raman spectra of the surface; c) Raman mappings of the studtite bands area and $2LO/T_{2g}$ area ratio. The scale of colors is indicated on the right (from blue for the lowest to red for the highest values); d) 3D surface reconstruction using the autofocus system. The white rectangle in a) indicates the mapping area.

Moreover, using the autofocus of the microscope (Figure 5d), it appears that after two leaching days the studtite-UO_2 areas are deeper than the sample's surface. This observation coincides with the increase in the U content in solution and shows that the UO_2 areas have dissolved first before the studtite precipitation, resulting in these holes at the surface of the pellet. This shows how the heterogeneities of the MOX samples affect the precipitation process. Not only the studtite did not precipitate on the plutonium-rich zones (coating phase and Pu agglomerates) after two days of leaching, but these zones did not, or only slightly, dissolve. This emphasizes the influence of the plutonium chemistry on the alteration of the MOX sample which increases the (U, Pu)O_2 matrix resistance to the dissolution.

At the end of the MOX leaching experiment, the studtite layer spread over almost the entire surface of the sample (Figure 6). While the UO_2 holes are now filled with studtite precipitates (white precipitation in the

SEM picture in Figure 6), a thin precipitation layer finally appeared on the Pu agglomerates. The Pu-rich areas are however still well preserved.

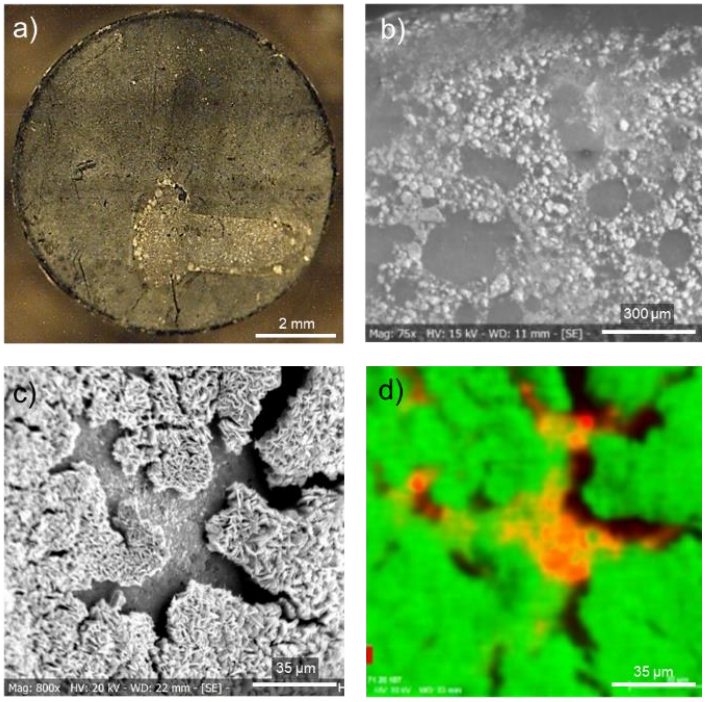

Figure 6 : MOX disc after 79 days of leaching a): Optical image reconstruction of the pellet's surface (5x, 24 images) in polarized light. b): SEM image at magnification 75x; c): SEM image of the area localized under the sample holder, 45° tilted sample, at magnification 800x. d) EDS mapping following the Pu (red) and U (green) signals associated to the c) area.

As visible on the photomicrograph of Figure 6, a "T" shape area stands out in the lower part of the pellet. It corresponds to the area that was located under the sample holder during the leaching in the reactor, and the precipitation is there more important. At high magnification (Figure 6c), we can recognize the needle-like precipitation characteristic of the studtite, but locally the layer is cracked. A MEB-EDS analysis (Figure 6d) following the U and Pu signals (respectively green and red scale) indicates that the matrix under these cracks is rich in plutonium, meaning that this studtite layer has also precipitated over a Pu agglomerate. By tilting the sample of 45° with respect to the detector, it appears that the precipitated layer, of around 3 µm thick, do not seems to adhere to the surface. In this localized confined area, the precipitation is favored, and a thick layer has developed, but contrary to the precipitation on the UO_2 grains the layer is distant from the sample surface.

These results highlight two effects: a confinement effect and a plutonium chemistry effect. First, the confinement of a small solution volume between the pellet and the sample holder has probably increased locally the concentration of U ions and radiolysis products, including H_2O_2, and thus promoted the precipitation under the sample holder. Second, and despite this local increase in precipitation, plutonium areas remain unfavorable precipitation sites as shown by the heterogeneous precipitation observed and the precipitated cracked area revealed by SEM suggesting a non-adherent precipitation onto the Pu rich zones.

3.5. Discussion on the leaching and precipitation mechanisms

The different isotopic enrichments observed for the uranyl ion and the peroxide bond during the first days of leaching leads to questioning the leaching processes (uranium oxidation and subsequent dissolution)

and the mechanisms of formation of the peroxide secondary phases. Indeed, it is not easy to understand for which reason ^{18}O enriched uranyl bond is mainly observed while the peroxide bond does not initially strongly exchange with ^{18}O.

Regarding the formation of studtite the precipitation process that is widely documented in the literature (with or without irradiation) [7,10,12,15] is classically described by the chemical reaction R1:

$$H_2O_2 + UO_2^{2+} + 4H_2O \Leftrightarrow UO_4.(4H_2O) + 2H^+ \qquad (R1)$$

The mechanisms of formation of the two main reactive species: hydrogen peroxide H_2O_2 and uranyl ion UO_2^{2+} must therefore be discussed.

a) Hydrogen peroxide H_2O_2 formation:

A quite simplistic approach would be to consider that the formation of hydrogen peroxide comes from the reaction between the $^{18}OH°$ radicals resulting from the radiolysis of $H_2{}^{18}O$ water molecules according to the reaction $^{18}OH° + {}^{18}OH° \longrightarrow H_2{}^{18}O_2$ (R2).

However, it should be recalled that under gamma irradiation, the measured hydrogen peroxide concentrations strongly depend on the nature of the gas phase. Thus, the presence of $^{16}O_2$ from the air (aerated conditions) leads to H_2O_2 contents in solution three orders of magnitude higher than those observed under argon. Dissolved oxygen ($^{16}O_2$) is a molecule that increases the decomposition of water because it efficiently scavenges electrons and H° radicals according to the reactions (R3) to (R6)[3]:

$$H° + {}^{16}O_2 \rightarrow HO_2° \qquad (R3)$$

$$e^-_{aq} + {}^{16}O_2 \rightarrow O_2^{°-} \qquad (R4)$$

$$HO_2° + O_2^{°-} (+H_2O) \rightarrow H_2O_2 + O_2 + OH^- \qquad (R5)$$

$$HO_2° + HO_2° \rightarrow H_2O_2 + O_2 \qquad (R6)$$

The radiolysis calculations associated with the experimental conditions and carried out according to the approach described by Jégou *et al.*[3] are in good agreement with the measured hydrogen peroxide concentrations and confirm a predominance of this chemical process. Indeed, for the gamma dose rate studied (~70 $Gy.h^{-1}$) the hydrogen peroxide concentration rapidly reaches a value of around 1.2×10^{-4} $mol.L^{-1}$ under air against 3×10^{-7} $mol.L^{-1}$ under argon. Therefore, for the aerated medium, the OH ° + OH ° reaction is not responsible primarily for the formation of hydrogen peroxide. In addition, it has been shown that ^{18}O enriched water does not easily exchange with a peroxide bond[42], which corroborates a predominant $H_2{}^{16}O_2$ isotopy during the first days under gamma irradiation.

b) Uranyl ion formation:

The presence of the uranyl ion into the solution results from the oxidation of the UO_2 matrix by water radiolysis products (oxidants like H_2O_2 and OH °radicals) and from the dissolution of this uranyl ion. On short times (< 1000 to 2000 hours), it was observed that uranyl ions retain the memory of the dissolution mechanism because the residence times of oxygen atoms in UO_2^{2+} ions are sufficiently long.[33] This point is a prerequisite for understanding and discussing the interfacial processes.

The work of Ekeroth[27] concluded that under gamma irradiation and in the presence of oxygen, the main oxidizing species responsible for the oxidation of UO_2 is H_2O_2 and not radicals. Their concentration is too low for them to have a kinetic effect even though they are thermodynamically more reactive (E° ($OH°$ / H_2O) = 2.7 VHNE > E° (H_2O_2 / H_2O) = 1.78 VNHE). In addition, the limiting step of the leaching mechanism is the oxidation of U(IV) to U(V) through a monoelectronic transfer (R7) followed by the formation of U(VI) (R8):

$$H_2O_2 + UO_{2(s)} \longrightarrow OH^{\circ} + OH^- + UO_{2(s)}^{+} \quad (R7)$$

$$OH^{\circ} + UO_{2(s)}^{+} \longrightarrow OH^- + UO_{2(s)}^{2+} \quad (R8)$$

According to Eriksen *et al.*[45], the OH° radical formed immediately reacts with U(V) to form U (VI) (R8). Such a process does not appear fully compatible with the results of our study because if H_2O_2 was the main reactive species involved in the formation of the uranyl ion, the process would mainly involve the ^{16}O isotope coming from the solid or from H_2O_2. This disagrees with the experimental isotopic signature of the uranyl ion. Moreover, recent work by Fidalgo *et al.*[46] have shown that the majority of hydrogen peroxide decomposes catalytically on the surface of fuels, which does not argue for a major participation in the oxidation of the surface. The surface-bound radicals formed by catalytic decomposition can also be scavenged by H_2O_2 which is produced here continuously without oxidizing the surface.[47]

It is more likely that H_2O_2 is not the main oxidant responsible for the formation of the uranyl ion but rather the $^{18}OH°$ radicals formed directly by the gamma radiolysis of enriched water, which would explain the difference in isotopy and exchanges. In 1992, Sunder[48] considered that radicals are responsible for the formation of U(V) by incorporation of interstitial oxygen atoms into the fluorite lattice according to the process (R9):

$$U(IV) + OH° \rightarrow H^+ + O_i^{2-} + U(V) \quad (R9)$$

The formation of the uranyl ion involves an additional $^{18}OH°$ radical.

Thus, the observed isotopic exchanges on the uranyl and peroxide bonds of the studtite precipitates of this leaching experiment would allow disclosing the origin of the main chemical species involved in the leaching mechanism. They suggest a strong role of the OH° radicals in the oxidation of the UO_2 matrix and formation of the uranyl bond, and of the hydrogen peroxide in the formation of the peroxide bond of the studtite.

Concerning the evolution over time of isotopies which tend towards “an equilibrium”, the chemical processes of H_2O_2 formation have no reason to evolve. However, the atoms in solution will exchange over long periods of time and the formation of dissolved oxygen with a different isotopy than that of the air will occur according to reactions:

$$O_2^{\circ-} + OH° \rightarrow O_2 + OH^- \quad (R10)$$

$$HO_2° + OH° \rightarrow O_2 + H_2O \quad (R11)$$

4. Conclusion

This study provides a better understanding of the oxidative dissolution of MOX fuels under gamma radiolysis of water as well as the precipitation of secondary phases. Under strong oxidizing conditions generated by gamma irradiation of an aerated water and for hydrogen peroxide concentrations around 10^{-4} mol.L^{-1}, the formation of uranium peroxide (studtite) is observed on the MOX fuel surface as for the UO_2 based fuel. No secondary plutonium-based phase is observed. This result illustrates the preferential dissolution of the UO_2 grains in the presence of oxidizing species, the zones with high plutonium contents being much more stable with respect to dissolution. In the early stages of the precipitation, this selective dissolution of the UO_2 grains leads to a local precipitation of studtite on their surface and in the corrosion pits, indicating a localized process at the interface. Local supersaturation processes are possible, these corrosion pits also being preferential germination sites. In the long term, the entire MOX fuel surface is covered, including the plutonium-enriched aggregates.

Concerning the formation of the uranyl ion and the peroxide bonds, isotopic analysis of the Raman bands of the studtite precipitates highlighted very distinct exchanges. The oxygen atoms in the uranyl bond and in the peroxide bond do not have the same origin, which could be explained by the respective roles of radicals and hydrogen peroxide. The radicals would be mainly involved in the formation of the uranyl ion during the fuel surface oxidation while the hydrogen peroxide would lead to the formation of peroxide bridges during the studtite precipitation. In the future, it will be necessary to confirm these results by working under alpha irradiation alone in order to assess the influence of the Linear Energy Transfer by promoting the formation of hydrogen peroxide from radicals and not from oxygen in the air. Finally, this work also demonstrates the feasibility of such an experimental approach, combining Raman imaging to isotopic labeling, to improve our understanding of dissolution mechanisms.

5. Acknowledgments

This study was funded by the CEA and EDF as part of the PRECCI research program. The authors thank the technicians from DHA-Atalante facility who strongly participated to this experiment: Loïck Chauvin, Nathalie Vaissières, Manuel Delaville and Maxime Fagard.

6. References

(1) Burns, P. C.; Ewing, R. C.; Navrotsky, A. Nuclear Fuel in a Reactor Accident. *Science (80-.).* **2012**, *335* (6073), 1184–1188. https://doi.org/10.1126/science.1211285.

(2) Grambow, B.; Poinssot, C. Interactions between Nuclear Fuel and Water at the Fukushima Daiichi Reactors. *Elements* **2012**, *8* (3), 213–219. https://doi.org/10.2113/gselements.8.3.213.

(3) Jégou, C.; Muzeau, B.; Broudic, V.; Peuget, S.; Poulesquen, A.; Roudil, D.; Corbel, C. Effect of External Gamma Irradiation on Dissolution of the Spent UO_2 Fuel Matrix. *J. Nucl. Mater.* **2005**, *341* (1), 62–82. https://doi.org/10.1016/j.jnucmat.2005.01.008.

(4) Nakayoshi, A.; Jegou, C.; De Windt, L.; Perrin, S.; Washiya, T. Leaching Behavior of Prototypical Corium Samples: A Step to Understand the Interactions between the Fuel Debris and Water at the Fukushima Daiichi Reactors. *Nucl. Eng. Des.* **2020**, *360*, 110522. https://doi.org/10.1016/j.nucengdes.2020.110522.

(5) Sunder, S.; Shoesmith, D. W.; Miller, N. H. Prediction of the Oxidative Dissolution Rates of Used Nuclear Fuel in a Geological Disposal Vault Due to the Alpha Radiolysis of Water. *MRS Proc.* **1994**, *353*, 617. https://doi.org/10.1557/PROC-353-617.

(6) Ewing, R. C. Long-Term Storage of Spent Nuclear Fuel. *Nat. Mater.* **2015**, *14* (3), 252–257. https://doi.org/10.1038/nmat4226.

(7) McNamara, B.; Buck, E.; Hanson, B. Observation of Studtite and Metastudtite on Spent Fuel. In *MRS Proceedings*; 2002; Vol. 757, p II9.7. https://doi.org/10.1557/PROC-757-II9.7.

(8) Hanson, B.; McNamara, B.; Buck, E.; Friese, J.; Jenson, E.; Krupka, K.; Arey, B. Corrosion of Commercial Spent Nuclear Fuel. 1. Formation of Studtite and Metastudtite. *Radiochim. Acta* **2005**, *93* (3), 159–168. https://doi.org/10.1524/ract.93.3.159.61613.

(9) McNamara, B.; Hanson, B. D.; Buck, E. C.; Soderquist, C. Corrosion of Commercial Spent Nuclear Fuel. 2. Radiochemical Analyses of Metastudtite and Leachates. *Radiochim. Acta* **2005**, *93* (3). https://doi.org/10.1524/ract.93.3.169.61615.

(10) Corbel, C.; Sattonnay, G.; Lucchini, J.-F.; Ardois, C.; Barthe, M.-F.; Huet, F.; Dehaudt, P.; Hickel, B.;

Jegou, C. Increase of the Uranium Release at an UO2/H2O Interface under He2+ Ion Beam Irradiation. *Nucl. Instruments Methods Phys. Res. Sect. B Beam Interact. with Mater. Atoms* **2001**, *179* (2), 225–229. https://doi.org/10.1016/S0168-583X(01)00519-5.

(11) Corbel, C.; Sattonnay, G.; Guilbert, S.; Garrido, F.; Barthe, M.-F.; Jegou, C. Addition versus Radiolytic Production Effects of Hydrogen Peroxide on Aqueous Corrosion of UO_2. *J. Nucl. Mater.* **2006**, *348* (1–2), 1–17. https://doi.org/10.1016/j.jnucmat.2005.05.009.

(12) Clarens, F.; de Pablo, J.; Díez-Pérez, I.; Casas, I.; Giménez, J.; Rovira, M. Formation of Studtite during the Oxidative Dissolution of UO 2 by Hydrogen Peroxide: A SFM Study. *Environ. Sci. Technol.* **2004**, *38* (24), 6656–6661. https://doi.org/10.1021/es0492891.

(13) Clarens, F.; de Pablo, J.; Casas, I.; Giménez, J.; Rovira, M.; Merino, J.; Cera, E.; Bruno, J.; Quiñones, J.; Martínez-Esparza, A. The Oxidative Dissolution of Unirradiated UO2 by Hydrogen Peroxide as a Function of PH. *J. Nucl. Mater.* **2005**, *345* (2–3), 225–231. https://doi.org/10.1016/j.jnucmat.2005.06.002.

(14) Burns, P. C.; Hughes, K.-A. Studtite, [(UO2)(O2)(H2O)2](H2O)2 : The First Structure of a Peroxide Mineral. *Am. Mineral.* **2003**, *88*, 1165–1168. https://doi.org/10.1016/j.cej.2016.03.019.

(15) Kubatko, K.-A. H. Stability of Peroxide-Containing Uranyl Minerals. *Science (80-.).* **2003**, *302* (5648), 1191–1193. https://doi.org/10.1126/science.1090259.

(16) Rey, A.; Casas, I.; Giménez, J.; Quiñones, J.; de Pablo, J. Effect of Temperature on Studtite Stability: Thermogravimetry and Differential Scanning Calorimetry Investigations. *J. Nucl. Mater.* **2009**, *385* (2), 467–473. https://doi.org/10.1016/j.jnucmat.2008.12.045.

(17) McGrail, B. T.; Sigmon, G. E.; Jouffret, L. J.; Andrews, C. R.; Burns, P. C. Raman Spectroscopic and ESI-MS Characterization of Uranyl Peroxide Cage Clusters. *Inorg. Chem.* **2014**, *53* (3), 1562–1569. https://doi.org/10.1021/ic402570b.

(18) Lobeck, H. L.; Isner, J. K.; Burns, P. C. Transformation of Uranyl Peroxide Studtite, [(UO 2)(O 2)(H 2 O) 2](H 2 O) 2 , to Soluble Nanoscale Cage Clusters. *Inorg. Chem.* **2019**, *58* (10), 6781–6789. https://doi.org/10.1021/acs.inorgchem.9b00230.

(19) Li, J.; Maier, A. C.; Jonsson, M. Stability of Studtite in Aqueous Suspension: Impact of HCO 3 – and Ionizing Radiation on the Dynamics of Dissolution. *ACS Appl. Energy Mater.* **2020**, *3* (1), 352–357. https://doi.org/10.1021/acsaem.9b01611.

(20) Rey, A.; Utsunomiya, S.; Gimenez, J.; Casas, I.; de Pablo, J.; Ewing, R. C. Stability of Uranium (VI) Peroxide Hydrates under Ionizing Radiation. *Am. Mineral.* **2009**, *94* (2–3), 229–235. https://doi.org/10.2138/am.2009.2908.

(21) Fairley, M.; Myers, N. M.; Szymanowski, J. E. S.; Sigmon, G. E.; Burns, P. C.; LaVerne, J. A. Stability of Solid Uranyl Peroxides under Irradiation. *Inorg. Chem.* **2019**, *58* (20), 14112–14119. https://doi.org/10.1021/acs.inorgchem.9b02132.

(22) Carbol, P.; Fors, P.; Van Winckel, S.; Spahiu, K. Corrosion of Irradiated MOX Fuel in Presence of Dissolved H2. *J. Nucl. Mater.* **2009**, *392* (1), 45–54. https://doi.org/10.1016/j.jnucmat.2009.03.044.

(23) Jégou, C.; Caraballo, R.; De Bonfils, J.; Broudic, V.; Peuget, S.; Vercouter, T.; Roudil, D. Oxidizing Dissolution of Spent MOX47 Fuel Subjected to Water Radiolysis: Solution Chemistry and Surface Characterization by Raman Spectroscopy. *J. Nucl. Mater.* **2010**. https://doi.org/10.1016/j.jnucmat.2010.01.004.

(24) Magnin, M.; Jégou, C.; Caraballo, R.; Broudic, V.; Tribet, M.; Peuget, S.; Talip, Z. Oxidizing Dissolution Mechanism of an Irradiated MOX Fuel in Underwater Aerated Conditions at Slightly Acidic PH. *J. Nucl. Mater.* **2015**, *462*, 230–241. https://doi.org/10.1016/j.jnucmat.2015.03.029.

(25) Guimbretière, G.; Desgranges, L.; Jegou, C.; Canizares, A.; Simon, P.; Caraballo, R.; Raimboux, N.; Barthe, M.-F.; Ammar, M.-R.; Maslova, O. A.; Duval, F.; Omnee, R. Characterization of Nuclear Materials in Extreme Conditions: Raman Spectroscopy Approach. *IEEE Trans. Nucl. Sci.* **2014**, *61* (4), 2045–2051. https://doi.org/10.1109/TNS.2014.2311166.

(26) Ekeroth, E.; Jonsson, M. Oxidation of UO2 by Radiolytic Oxidants. *J. Nucl. Mater.* **2003**, *322* (2–3), 242–248. https://doi.org/10.1016/j.jnucmat.2003.07.001.

(27) Ekeroth, E.; Roth, O.; Jonsson, M. The Relative Impact of Radiolysis Products in Radiation Induced Oxidative Dissolution of UO2. *J. Nucl. Mater.* **2006**, *355* (1–3), 38–46. https://doi.org/10.1016/j.jnucmat.2006.04.001.

(28) Oudinet, G.; Munoz-Viallard, I.; Aufore, L.; Gotta, M. J.; Becker, J. M.; Chiarelli, G.; Castelli, R. Characterization of Plutonium Distribution in MIMAS MOX by Image Analysis. *J. Nucl. Mater.* **2008**. https://doi.org/10.1016/j.jnucmat.2007.10.013.

(29) Roth, O.; Jonsson, M. Oxidation of $UO_{2(s)}$ in Aqueous Solution. *Cent. Eur. J. Chem.* **2008**, *6* (1), 1–14. https://doi.org/10.2478/s11532-007-0067-z.

(30) Bastians, S.; Crump, G.; Griffith, W. P.; Withnall, R. Raspite and Studtite: Raman Spectra of Two Unique Minerals. *J. Raman Spectrosc.* **2004**, *35* (89), 726–731. https://doi.org/10.1002/jrs.1176.

(31) Weck, P. F.; Kim, E.; Jové-Colón, C. F.; Sassani, D. C. Structures of Uranyl Peroxide Hydrates: A First-Principles Study of Studtite and Metastudtite. *Dalt. Trans.* **2012**, *41* (32), 9748–9752. https://doi.org/10.1039/c2dt31242e.

(32) Brooker, M. H.; Huang, C. B.; Sylwestrowicz, J. Raman Spectroscopic Studies of Aqueous Uranyl Nitrate and Perchlorate Systems. *J. Inorg. Nucl. Chem.* **1980**, *42* (10), 1431–1440. https://doi.org/10.1016/0022-1902(80)80109-6.

(33) Berger, P. Etude Du Mécanisme de La Dissolution Par Oxydoreduction Chimique et Electrochimique Des Bioxydes d'actinides (UO2, NpO2, PuO2, AmO2) En Milieu Aqueux Acide, Université Paris VI, 1990.

(34) Nguyen-Trung, C.; Begun, G. M.; Palmer, D. A. Aqueous Uranium Complexes. 2. Raman Spectroscopic Study of the Complex Formation of the Dioxouranium(VI) Ion with a Variety of Inorganic and Organic Ligands. *Inorg. Chem.* **1992**, *31* (25), 5280–5287. https://doi.org/10.1021/ic00051a021.

(35) Lu, G.; Haes, A. J.; Forbes, T. Z. Detection and Identification of Solids, Surfaces, and Solutions of Uranium Using Vibrational Spectroscopy. *Coord. Chem. Rev.* **2018**, *374*, 314–344. https://doi.org/10.1016/j.ccr.2018.07.010.

(36) Faulques, E.; Massuyeau, F.; Kalashnyk, N.; Perry, D. L. Application of Raman and Photoluminescence Spectroscopy for Identification of Uranium Minerals in the Environment. *Spectrosc. Eur.* **2015**, *27* (1), 14–25.

(37) Vacque, V.; Sombret, B.; Huvenne, J. P. P.; Legrand, P.; Suc, S. Characterisation of the O-O Peroxide Bond by Vibrational Spectroscopy. *Spectrochim. Acta Part A Mol. Biomol. Spectrosc.* **2002**, *53* (1), 55–66. https://doi.org/10.1016/s1386-1425(97)83009-0.

(38) Lv, J.; Li, G.; Guo, S.; Shi, Y. Raman Scattering from Phonons and Electronic Excitations in UO_2 with

Different Oxygen Isotopes. *J. Raman Spectrosc.* **2015**, *47* (3), 345–349. https://doi.org/10.1002/jrs.4785.

(39) Xu, M.; Traustason, H.; Bo, F. D.; Hickam, S.; Chong, S.; Zhang, L.; Oliver, A. G.; Burns, P. C. Supramolecular Assembly of Geometrically Unstable Hybrid Organic–Inorganic Uranyl Peroxide Cage Clusters and Their Transformations. *J. Am. Chem. Soc.* **2019**, *141* (32), 12780–12788. https://doi.org/10.1021/jacs.9b05599.

(40) Gordon, G.; Taube, H. Isotopic Tracer Studies on the Thermal Decomposition of Uranium Peroxide. *J. Inorg. Nucl. Chem.* **1961**, *16* (3–4), 268–271. https://doi.org/10.1016/0022-1902(61)80501-0.

(41) Anbar, M.; Guttmann, S. The Exchange of Oxygen between Hydrogen Peroxide and Water in Nitric Acid Solutions. *J. Am. Chem. Soc.* **1961**, *83* (9), 2035–2037. https://doi.org/10.1021/ja01470a002.

(42) Lonadier, F. D.; Boggs, J. E. Isotope Exchange Studies on the Uranium(vi) Oxide Hydrates and Uranium Peroxide. *J. Less-Common Met.* **1963**, *5* (2), 112–116. https://doi.org/10.1016/0022-5088(63)90003-1.

(43) Talip, Z.; Peuget, S.; Magnin, M.; Berardo, L.; Valot, C.; Vauchy, R.; Jégou, C. Raman Microspectroscopic Studies of Unirradiated Homogeneous (U0.76Pu0.24)O2+x: The Effects of Pu Content, Non-Stoichiometry, Self-Radiation Damage and Secondary Phases. *J. Raman Spectrosc.* **2017**, *48* (5), 765–772. https://doi.org/10.1002/jrs.5092.

(44) Böhler, R.; Welland, M. J.; Prieur, D.; Cakir, P.; Vitova, T.; Pruessmann, T.; Pidchenko, I.; Hennig, C.; Guéneau, C.; Konings, R. J. M.; Manara, D. Recent Advances in the Study of the UO_2-PuO_2 Phase Diagram at High Temperatures. *J. Nucl. Mater.* **2014**, *448*, 330–339. https://doi.org/10.1016/j.jnucmat.2014.02.029.

(45) Eriksen, T. E.; Shoesmith, D. W.; Jonsson, M. Radiation Induced Dissolution of UO_2 Based Nuclear Fuel – A Critical Review of Predictive Modelling Approaches. *J. Nucl. Mater.* **2012**, *420* (1–3), 409–423. https://doi.org/10.1016/j.jnucmat.2011.10.027.

(46) Barreiro Fidalgo, A.; Jonsson, M. Radiation Induced Dissolution of (U, Gd)O_2 Pellets in Aqueous Solution – A Comparison to Standard UO_2 Pellets. *J. Nucl. Mater.* **2019**, *514*, 216–223. https://doi.org/10.1016/j.jnucmat.2018.11.037.

(47) Barreiro Fidalgo, A.; Kumagai, Y.; Jonsson, M. The Role of Surface-Bound Hydroxyl Radicals in the Reaction between H 2 O 2 and UO 2. *J. Coord. Chem.* **2018**, *71* (11–13), 1799–1807. https://doi.org/10.1080/00958972.2018.1466287.

(48) Sunder, S.; Shoesmith, D. W.; Christensen, H.; Miller, N. H. Oxidation of UO2 Fuel by the Products of Gamma Radiolysis of Water. *J. Nucl. Mater.* **1992**, *190*, 78–86. https://doi.org/10.1016/0022-3115(92)90078-Y.

(49) Schumb, W. C. Stability of Concentrated Hydrogen Peroxide Solutions. *Ind. Eng. Chem.* **1949**, *41* (5), 992–1003. https://doi.org/10.1021/ie50473a026.

(50) Hiroki, A.; LaVerne, J. A. Decomposition of Hydrogen Peroxide at Water-Ceramic Oxide Interfaces. *J. Phys. Chem. B* **2005**, *109* (8), 3364–3370. https://doi.org/10.1021/jp046405d.